

# Structural Evolution of Pd-Doped Nanoscale Zero-Valent Iron (nZVI) in Aqueous Media and Implications for Particle Aging and Reactivity

WEILE YAN,<sup>†</sup> ANDREW A. HERZING,<sup>\*,§</sup>  
XIAO-QIN LI,<sup>†</sup> CHRISTOPHER J. KIELY,<sup>‡</sup>  
AND WEI-XIAN ZHANG<sup>\*,†,||</sup>

Department of Civil and Environmental Engineering, Lehigh University, Bethlehem, Pennsylvania 18015, Department of Materials Science and Engineering, Lehigh University, 5 East Packer Avenue, Bethlehem, Pennsylvania 18015-3195, Surface and Microanalysis Science Division, National Institute of Standards and Technology, 100 Bureau Drive, Mailstop 8371, Gaithersburg, Maryland 20899-8371, and State Key Laboratory for Pollution Control & Resources Reuse, Tongji University, Shanghai 200092, People's Republic of China

Received February 15, 2010. Revised manuscript received April 8, 2010. Accepted April 21, 2010.

Palladized zero-valent iron nanoparticles have been frequently employed to achieve enhanced treatment of halogenated organic compounds; however, no detailed study has been published on their structures, especially the location and distribution of palladium within the nanoparticles. In this work, the structural evolution of palladized nanoscale iron particles (Pd–nZVI, with 1.5 wt % Pd) was examined using X-ray photoelectron spectroscopy (XPS), scanning transmission electron microscopy (STEM), and X-ray energy dispersive spectroscopy (XEDS) techniques. The STEM-XEDS technique enables direct visualization of the nanoscale structural and compositional changes of the bimetallic particles. For a freshly made Pd–nZVI sample, the particles consist of a metallic iron core and a thin amorphous oxide shell, and Pd is observed to form 2–5 nm islands decorating the outer surface of the nanoparticles. Upon exposure to water, Pd–nZVI undergoes substantial morphological and structural changes. STEM-XEDS elemental maps show that Pd infiltrates through the oxide layer to the metallic iron interface, which is accompanied by oxidation and outward diffusion of the iron species. Within a 24 h period, Pd is completely buried underneath an extensive iron oxide matrix, and a fraction of the nanoparticles exhibits a hollowed-out morphology with no metallic iron remaining. The microstructural variations observed concur with the reactivity data, which shows that the aged bimetallic particles display an 80% decrease in dechlorination rate of trichloroethene (TCE) compared to that of the fresh particles. These findings

shed new light on the function of palladium in hydrodechlorination reactions, nZVI aging and deactivation, and the longevity of Pd–nZVI nanoparticles for in situ remediation.

## Introduction

Nanoscale zero-valent iron (nZVI) represents the most widely studied engineered nanomaterials in environmental remediation and toxic waste treatment. The reactivity of nZVI can be substantially improved by impregnating with a second metal, typically Pd, Pt, Ni, Ag, or Cu, to form so-called bimetallic nanoparticles. Among these transition metal additives, Pd-doped nZVI (Pd–nZVI) is known to exhibit higher reactivity than the other reported bimetallic systems (1, 2). For treatment of chlorinated organic compounds (e.g., trichloroethene and tetrachloroethene), Pd–Fe bimetallic materials yield more saturated products (e.g., C<sub>2</sub>H<sub>6</sub>) and generate less toxic intermediates, such as dichloroethenes and vinyl chloride, which are often produced in significant amounts with monometallic iron (1, 3). Ample literature exists on reductive dehalogenation using nanosized Pd–Fe bimetallic materials, and Table 1 summarizes some of the most frequently cited laboratory and field studies (4–13).

Palladium metal is a well-known heterogeneous catalyst for gas-phase dehalogenation and hydrogenation reactions (1, 14). The use of Pd-impregnated iron (Pd–Fe) for groundwater remediation is a relatively recent application. Mechanistic studies of the degradation of simple aliphatic chlorinated compounds in water suggest that the iron component of the Pd–Fe material serves as the source of electrons, whereas palladium behaves as a catalyst for hydrogen formation, activation, and the subsequent formation of dissociated hydrogen species, which in turn act as the reducing agents responsible for the dechlorination and hydrogenation of the contaminants (2, 3, 15). In contrast to gas-phase reactions, the use of iron materials in water remediation inevitably requires that they sustain prolonged contact with the aqueous environment and undergo reactions with water. Moreover, in the presence of Pd, the reaction of Fe with water is accelerated due to the galvanic effect between iron and palladium in addition to the well-known ability of the latter to catalytically promote water reduction and hydrogen generation (2, 15). Because of the large excess of water molecules relative to those contaminants of concern, the interaction of the Pd–Fe particles with water determines the longevity of these materials and their long-term effectiveness for contaminant remediation. Stability in water is particularly important for nanoscale, Fe-based materials due to the enhanced reactivity imparted by their large surface area. While the aging behavior of monometallic nZVI has been examined (16, 17), few studies have been conducted to investigate the effect of aqueous exposure on the structure and composition of these bimetallic nanoparticles (13, 18).

In this work, state-of-the-art X-ray energy dispersive spectroscopy (XEDS) spectrum imaging in an aberration-corrected scanning transmission electron microscope (STEM) (19–22) is utilized for high resolution elemental mapping of Pd–nZVI bimetallic nanoparticles. The STEM-XEDS technique enables direct visualization of the nanoscale structural and compositional changes of the bimetallic particles induced by their aging in water. These findings are correlated with the results from X-ray photoelectron spectroscopy (XPS) and batch experiments with trichloroethene (TCE) in an effort to generate a more complete understanding of the reactivity and stability of Pd–nZVI particles in aqueous media over

\* Corresponding author phone: 1-610-758-5318; fax: 1-610-758-6405; e-mail: wez3@lehigh.edu.

<sup>†</sup> Department of Civil and Environmental Engineering, Lehigh University.

<sup>‡</sup> Department of Materials Science and Engineering, Lehigh University.

<sup>§</sup> National Institute of Standards and Technology.

<sup>||</sup> Tongji University.

**TABLE 1. Common Halogenated Contaminants Treated by Pd–Fe Bimetallic Nanoparticles in Recent Studies**

contaminant	Pd–Fe materials	reference
chlorinated methanes tetrachloroethene (PCE), trichloroethene (TCE), <i>cis</i> -dichloroethene ( <i>cis</i> -DCE), vinyl chloride (VC) trichloroethene (TCE)	as synthesized Pd(0.05–1% by mass)–Fe nanoparticles	4
	as-synthesized Pd–Fe nanoparticles	5
	Pd(10% by mass)–Fe nanoparticles embedded in PAA/PES membrane	6
	Starch stabilized Pd(0.1% by mass)–Fe nanoparticles as-synthesized Pd(0.3% by mass)–Fe nanoparticles for field evaluation	7 8, 9
chlorophenols	encapsulated Pd–Fe in magnetic stabilized fluid bed reactor	10
polychlorinated biphenyls (PCB)	as-synthesized Pd–Fe nanoparticles	11
	as-synthesized Pd(0.68% by mass)–Fe on granular activated carbon support	12
chlorobenzenes	as-synthesized Pd(0.1% by mass)–Fe nanoparticles and particles regenerated by acid or NaBH <sub>4</sub>	13

time, and the implications of these results for water treatment and remediation are discussed.

## Materials and Methods

**Preparation of Nanoparticles.** Iron nanoparticles (nZVI) were prepared using a sodium borohydride reduction method as described previously (23, 24). Pd–Fe bimetallic nanoparticles (Pd–nZVI) were prepared by reacting the freshly prepared iron nanoparticles with an ethanol/water (vol. ratio 1:1) solution of palladium chloride. In this study, the nominal loading of Pd with respect to iron was fixed at a mass fraction of 1.5%. More details on the nanoparticle synthesis are available in Supporting Information.

**Aging Experiments.** The aging experiment was performed in 120-mL serum bottles containing 100 mL of deionized water. An appropriate amount of freshly made nZVI or Pd–nZVI nanoparticles were added into 100 mL of DI water to reach a concentration of 5 g/L. The bottles were sealed with crimp caps having a Teflon-lined septum and placed on a mechanical shaker at 25 °C for 24 h. The solid residues were harvested by vacuum filtration and dried in a glovebag containing high purity N<sub>2</sub> before high-resolution X-ray photoelectron spectroscopy (HR-XPS) analysis.

**Surface Analysis.** HR-XPS analysis was performed on a Scienta ESCA 300 spectrometer equipped with a rotating Al anode generating Al K<sub>α</sub> X-ray radiation at 1486.7 eV. Samples were analyzed at C 1s, O 1s, Fe 2p, and Pd 3d regions after survey scans. More details on XPS procedure are provided in Supporting Information.

**Electron Microscopy Analysis.** Electron microscopy analysis was performed immediately after the fresh or aged nanoparticles were prepared. High-angle annular dark-field (HAADF) imaging and XEDS spectrum imaging were performed using an FEI Titan 80–300 TEM/STEM operating at 300 kV in scanning (STEM) mode. This instrument is equipped with a double-hexapole spherical aberration (C<sub>s</sub>) corrector (CEOS GmbH) and an EDAX r-TEM system for XEDS analysis.

The details of XEDS spectrum imaging have been described elsewhere (19–21). Briefly, the electron probe is slowly scanned over a two-dimensional area of interest, collecting an entire X-ray fluorescence spectrum at each pixel. Because the aberration-corrected STEM probe is only about 100 pm in diameter, this type of analysis can be carried out at very high spatial resolution. In the present case, the data was collected at a pixel size of 1 nm<sup>2</sup> or less. The end result of this acquisition is a spectrum image data cube defined by the spatial coordinates of the pixels (*x* and *y*) and the energy channels of the XEDS spectra (*E*). Postprocessing of the data-cube generates individual elemental maps and overlay compositional maps. More details on XEDS spectrum imaging are available in Supporting Information.

**Batch Experiments.** TCE dechlorination experiments were conducted to compare the reactivity of fresh and aged Pd–nZVI particles. To remove hydrogen species accumulated in the solid phase during the aging process, which may contribute to TCE dechlorination, the aged nZVI suspension was sonicated for 10 min in air before collection by vacuum filtration and use in the subsequent TCE batch experiments. At the beginning of each experiment, a 100 mL of aqueous TCE solution (50 mg/L) was charged into a 250-mL serum bottle containing 0.25 g Pd–nZVI. The bottle was capped with a Teflon Mininert valve and mixed on a mechanical shaker at 250 rpm at room temperature (25 °C). Periodically, a 25- $\mu$ L aliquot of headspace gas was withdrawn using a gastight syringe for gas chromatography (GC) analysis. The concentration of TCE was measured by a Shimadzu GC analyzer (GC-17A) equipped with a flame ionization detector and a Supelco SPB 624 capillary column. A blank experiment was performed in parallel under identical conditions but without the addition of Pd–nZVI particles.

## Results and Discussion

**Surface Chemistry Analysis with XPS.** Figures 1a and 1b show the Fe 2p XPS spectra of the nZVI and Pd–nZVI materials, respectively. The two spectra correspond to the freshly made nanoparticles and those aged in water for 24 h. The Fe 2p<sub>3/2</sub> photoelectron peaks at 706.6 and 710.8 eV can be assigned to metallic iron (Fe(0)) and oxidized iron (Fe(III)) based on the binding energies (B.E.) (23). For the freshly made nZVI and Pd–nZVI particles, a strong Fe(III) peak was present along with a relatively small Fe(0) peak. Considering that the typical sampling depth of the XPS technique for metal oxides is less than 10 nm (23), the Fe spectra agree with the core–shell model described in the literature, in which a metallic iron core is surrounded by a thin layer of oxidized iron. The overlayer is thought to form spontaneously upon synthesis in an aqueous solution (24, 25). Prior analysis of O 1s spectra of freshly made nZVI suggests that the oxide phase has a stoichiometry of iron oxyhydroxide (FeOOH) (24). The relative abundances of Fe(0) to Fe(III) are comparable for the nZVI and Pd–nZVI materials, suggesting that the Pd impregnation process does not cause a significant alteration to the core–shell structure.

After the nanoparticles were aged in water for 24 h, the Fe(0) peak remains observable for the undoped Fe nanoparticles (Figure 1a). However, its decreased intensity indicates that surface corrosion may have occurred, effectively increasing the shell thickness during the aging process. In contrast, the Pd–nZVI nanoparticles immersed in water for one day did not exhibit any metallic iron component in the XPS spectrum (Figure 1b), implying that the particles had undergone more severe oxidation during the aging process. Figure 1c shows the Pd 3d XPS spectra of

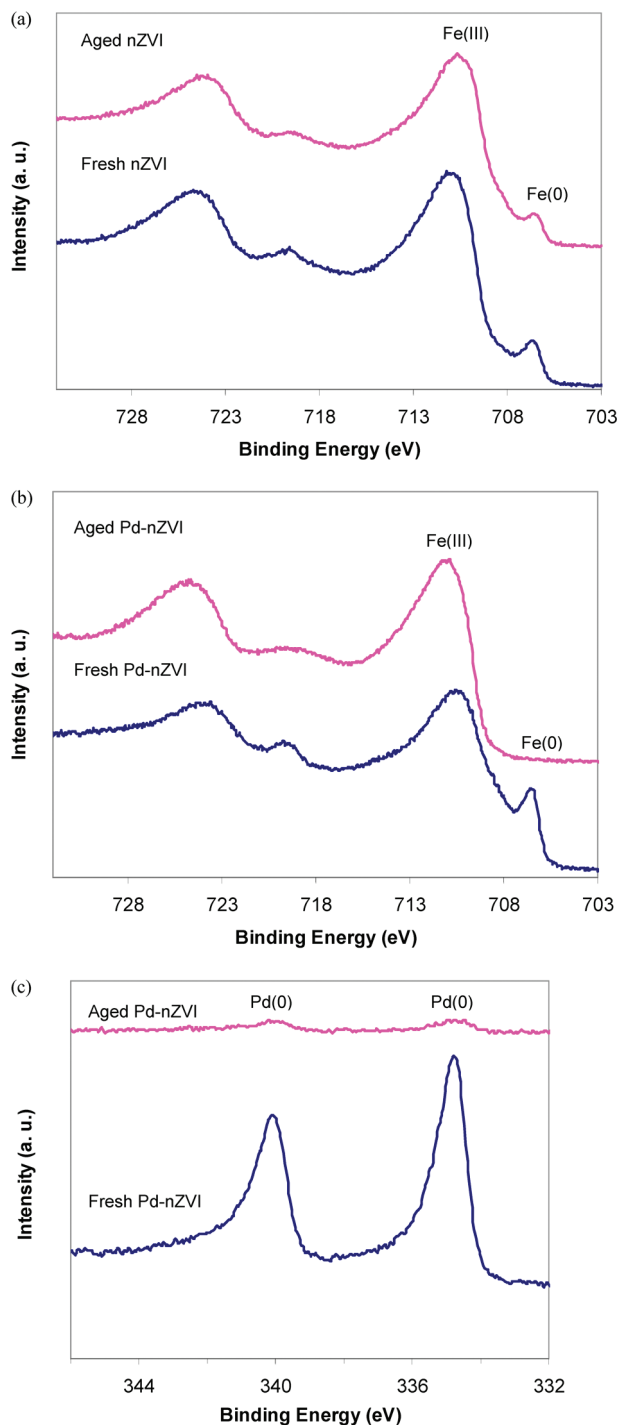


**FIGURE 1.** Fe 2p XPS spectra of (a) monometallic iron nanoparticles (nZVI) and (b) Pd-impregnated iron nanoparticles (Pd-nZVI). (c) Pd 3d spectra of Pd-nZVI. The spectra in blue represent freshly made nanoparticles, while those in pink are for particles aged in aqueous media for 24 h.

the freshly made and the aged Pd-nZVI materials. The fresh Pd-nZVI exhibits two prominent peaks with binding energies of 334.7 and 340.0 eV, respectively. The positions and the peak shape match with the  $3d_{5/2}$  and  $3d_{3/2}$  peaks for Pd(0) (18). No other Pd valence state was observed, thus confirming that the impregnated Pd was completely reduced to Pd(0) via a Pd(II)-Fe(0) replacement reaction. However, after a one-day exposure to an aqueous environment, the Pd  $3d_{5/2}$  and  $3d_{3/2}$  signals were severely attenuated and barely discernible from the background noise. Analysis of the solution in which Pd-nZVI particles were suspended showed

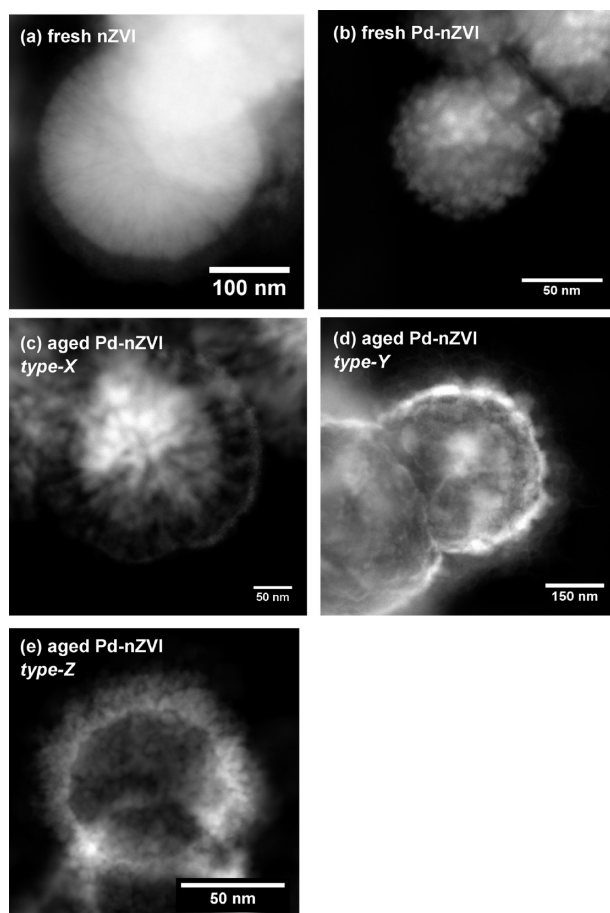


**FIGURE 2.** HAADF images of iron nanoparticles: (a) fresh monometallic nZVI; (b) fresh Pd-nZVI; (c-e) Pd-nZVI after aqueous aging for 24 h.

no elution (<0.1 wt.%) of Pd into the aqueous phase, suggesting that Pd may have become effectively buried underneath a growing layer of iron corrosion products during the 24-h period. The combined results of Fe 2p and Pd 3d XPS analysis suggest crucial location changes for palladium in the bimetallic particles after exposure to water.

**Microscopic Characterization and Interpretation of Structural Evolution.** Figure 2 presents a series of high-angle annular dark field (HAADF) images of undoped nZVI and palladized nZVI (Pd-nZVI) particles. The signal collected via the HAADF imaging technique is sensitive to atomic number, and heavier elements scatter more efficiently onto the high collection angle detector employed. Thus, the regions of the specimen with greater average through-thickness atomic number will appear brighter. The particle in Figure 2a consists of a bright core, corresponding to metallic iron, enclosed by a shell of lower intensity, which is thought to be iron oxide. Previous combined TEM and XPS studies (23, 24) have identified the core of the nZVI particle to consist of nanocrystalline (*bcc*) metallic Fe, while the shell is a highly disordered iron oxyhydroxide (FeOOH) layer. This structural identification is further verified by the TEM images (Supporting Information, Figure S1a,b) and Fe  $K_{\alpha}$  and O  $K_{\alpha}$  STEM-XEDS compositional maps (Supporting Information, Figure S1c,d), where there is a reduced intensity Fe signal and a much enhanced O signal in the FeOOH overlayer region. The color overlay of the Fe and O signals (Supporting Information, Figure S1e) clearly illustrates the core-shell structure of the nZVI particle.

Figure 2b shows a HAADF image of a typical particle morphology found in the freshly prepared Pd-nZVI material. When compared to the undoped nZVI (Figure 2a), the fresh

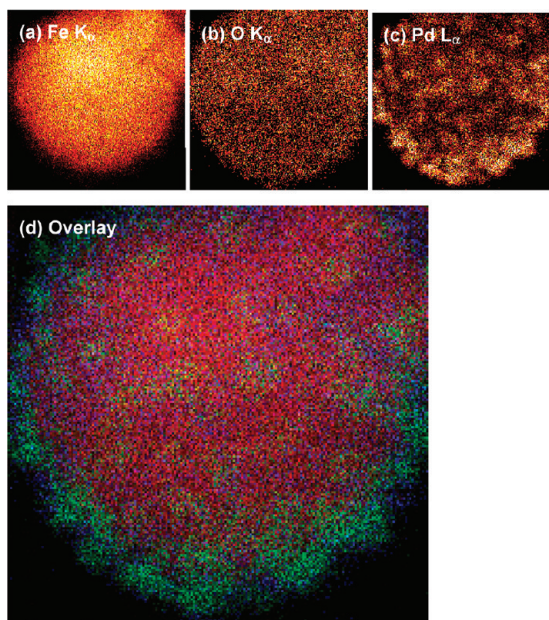
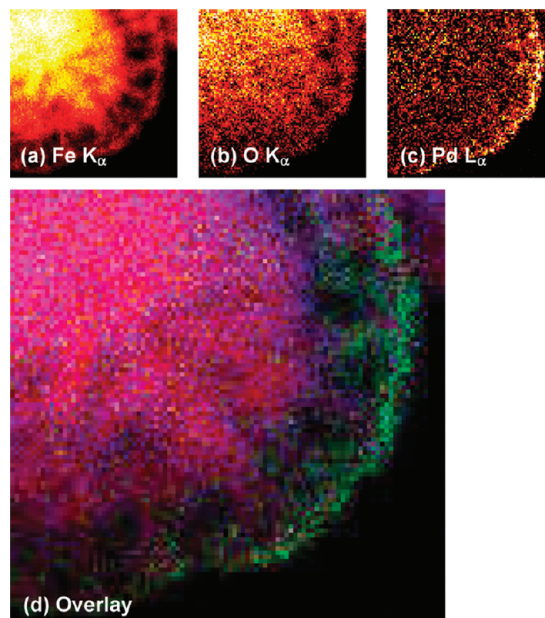


**FIGURE 3.** STEM-XEDS elemental maps of the Fe  $K_{\alpha}$  (a), O  $K_{\alpha}$  (b), and Pd  $L_{\alpha}$  (c) X-ray signals collected from the fresh Pd-nZVI particle shown in Figure 2b. A color overlay (d) emphasizes the spatial extent of each signal (red = Fe, blue = O, and green = Pd).

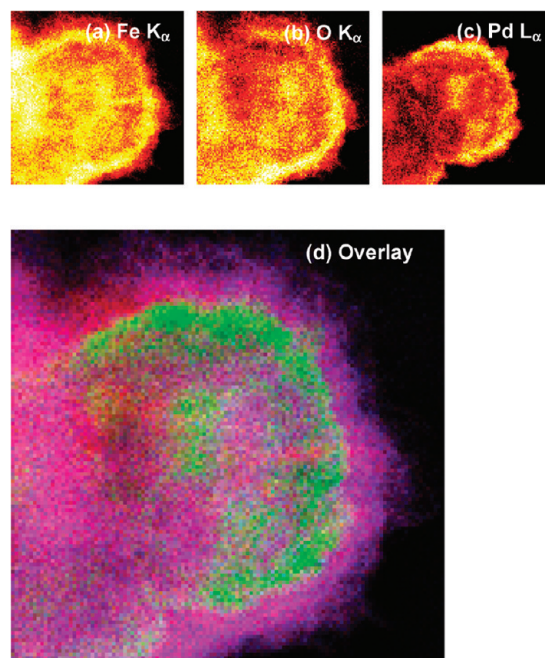
Pd-nZVI particles have a considerably rougher surface profile, and the surface is decorated with 2–5 nm particles. After exposure to water for 24 h, the Pd-nZVI particles undergo gross morphological changes as evidenced in the three HAADF images presented in Figure 2c–e. The starting Pd-nZVI structure and the three coexisting ‘water-aged’ morphologies (labeled X, Y, and Z) can be interpreted more fully when considered in conjunction with their corresponding STEM-XEDS elemental maps, which are presented in Figures 3–6. Each set of STEM-XEDS maps consists of individual elemental maps for Fe  $K_{\alpha}$ , O  $K_{\alpha}$ , and Pd  $L_{\alpha}$ , and a color overlay map of the three elements.

Figure 3 (and additional images in Figure S2, Supporting Information) shows STEM-XEDS mapping data from the typical morphologies found in the fresh Pd-nZVI sample. Figure 3a–c show the Fe  $K_{\alpha}$ , O  $K_{\alpha}$ , and Pd  $L_{\alpha}$  elemental maps acquired from the particle shown previously in Figure 2b. The Pd  $L_{\alpha}$  map confirms that the brighter nanosized features in HAADF image are indeed Pd clusters. The XPS spectra acquired from the fresh Pd-nZVI sample (Figure 1c) suggest that these are metallic rather than oxidized Pd nanoparticles. The color overlay of the three maps (Figure 3d), where the elemental distributions of Fe, O, and Pd are represented in red, blue and green, respectively, clearly highlights the discrete Pd nanoclusters decorating the surface of the Fe/oxide core-shell particle.

Figure 4 shows the Fe  $K_{\alpha}$ , O  $K_{\alpha}$ , and Pd  $L_{\alpha}$  STEM-XEDS elemental maps from the ‘after -aging’ morphology, which is denoted as type-X in Figure 2c. Close examination of Figure 4c,d suggests that the Pd is beginning to penetrate through the less dense oxide outerlayer toward the metallic Fe core. The elemental maps corresponding to the ‘after-aging’ morphology denoted as type-Y in Figure 2d are presented in Figure 5. The spatial extent of the Pd signal (Figure 5c) is found to be considerably smaller than that of the Fe signal (Figure 5a), suggesting that the Pd in this particle is now all subsurface. The color overlay of elemental maps (Figure 5d) demonstrates the situation where all Pd is accumulating as a buried (green) layer at the metallic Fe/oxide interface. This observation of a buried interfacial layer of Pd is consistent



**FIGURE 4.** STEM-XEDS elemental maps of the Fe  $K_{\alpha}$  (a), O  $K_{\alpha}$  (b), and Pd  $L_{\alpha}$  (c) X-ray signals collected from the type-X aged Pd-nZVI particle shown in Figure 2c. A color overlay (d) emphasizes the spatial extent of each signal (red = Fe, blue = O, and green = Pd).



**FIGURE 5.** STEM-XEDS elemental maps of the Fe  $K_{\alpha}$  (a), O  $K_{\alpha}$  (b), and Pd  $L_{\alpha}$  (c) X-ray signals collected from the type-Y aged Pd-nZVI particle shown in Figure 2d. A color overlay (d) emphasizes the spatial extent of each signal (red = Fe, blue = O, and green = Pd).

with the XPS data, where a dramatic decrease in overall surface Pd signal was noted for the samples aged in water (Figure 1c).

The third distinct (type-Z) morphology of aged Pd-nZVI particle (Figure 2e), shows a characteristic low level of contrast at its center the HAADF image, suggesting that it may in fact have a hollow core. Figure 6 shows the corresponding STEM-XEDS elemental data for this particle type. The Fe  $K_{\alpha}$  and O  $K_{\alpha}$  elemental maps (Figure 6a and Figure 6b, respectively) show a very close correspondence, suggesting that complete

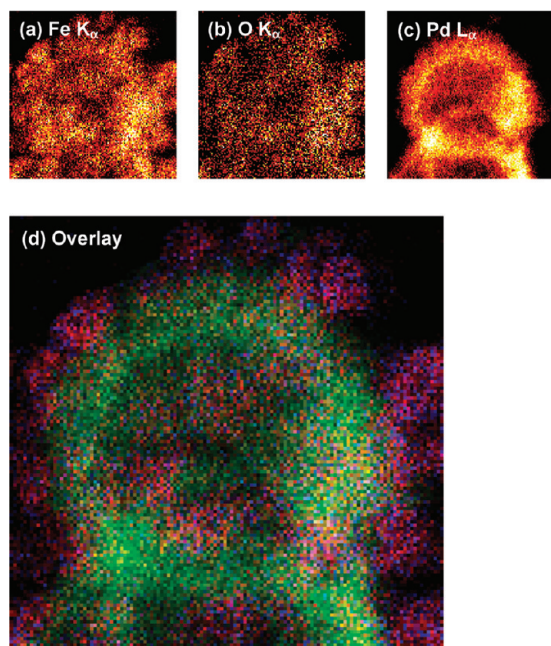


**FIGURE 6.** STEM-XEDS elemental maps of the Fe  $K_{\alpha}$  (a), O  $K_{\alpha}$  (b), and Pd  $L_{\alpha}$  (c) X-ray signals collected from the type-Z aged Pd-nZVI particle shown in Figure 2e. A color overlay (d) emphasizes the spatial extent of each signal (red = Fe, blue = O, and green = Pd).

oxidation of metallic iron has occurred, and both display an intensity decrease at the particle center indicative of the presence of a central void. The Pd distribution shown in Figure 6c indicates that the Pd is located under the oxide layer, seemingly defining the interior surface of the pore. We believe that while the Pd is diffusing inward to the Fe/oxide interface, the metallic Fe associated with the core simultaneously diffuses outward, oxidizes, and contributes to the FeOOH external shell, which then grows in thickness until eventually all the metallic Fe is consumed. This oxidation process could be controlled by several factors, including the particle surface area, exposure of different surface crystallographic facets, and the amount of Pd decorating the surface. Therefore, the microstructural heterogeneities in the system cause the reaction rate to vary from particle-to-particle, and we observe multiple types of microstructure (X, Y, and Z) in the aged sample. The progression from one morphology to the next cannot be unequivocally addressed in this study, since our structural characterization was carried out at only one aging interval (24 h). However, our interpretation of the data is that during exposure to water, nZVI particles, which originally have Pd on their outer surfaces, sequentially transform through the X, Y, and Z microstructures that have been identified in this study.

The structural changes observed due to aging, namely, the increase in oxide layer thickness, the enclosure of the initial surface Pd by the oxide layer, and in some cases the evacuation of the metallic iron core to give a characteristic “hollowed-out” structure, may result from several processes. The growth of the oxide layer is the net result of iron oxidation, outward diffusion of Fe(II), and oxidation and precipitation of Fe(II) upon reactions with water, dissolved oxygen, and other potential oxidants in the solution phase (26). Similar phenomena including the outward diffusion of the metal species and the growth of an oxide shell have been observed previously during the oxidation of iron and cobalt nanoparticles in gas or aqueous media (26, 27). The inward migration of palladium metal is also favored thermodynamically since the core region has the highest concentration of metallic iron, which reduces Pd(II) and stabilizes elemental

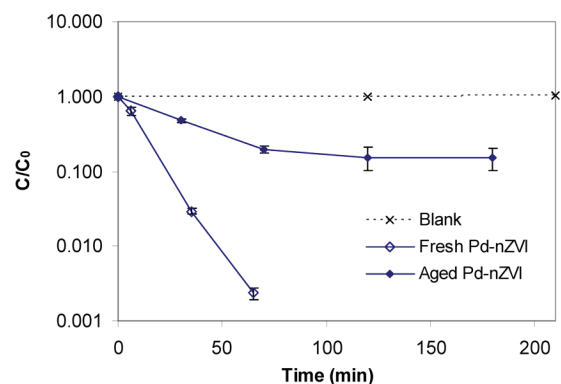


**FIGURE 7.** TCE removal by fresh or aged Pd-nZVI particles. Initial TCE concentration was 50 mg/L, and particle dose was 2.5 g/L. The error bars represent the results of duplicate runs.

palladium. Due to the very large surface-area-to-volume ratio and short diffusion distances associated with these nanoscale particles, the mass transport could easily result in void formation and eventually a hollow structure within reasonably short time frames.

In the case of Pd-nZVI, the process of iron oxidation is significantly accelerated compared to the undoped nZVI particles. The effect is attributed to the galvanic contact between palladium and iron, which creates a large electrochemical potential difference ( $\Delta E^{\circ} = 1.355$  V) (28) driving iron oxidation. In addition, palladium is also a well-known hydrogenation catalyst (14) for water reduction to hydrogen. Both effects result in enhanced iron corrosion. Our experiments to evaluate the hydrogen generation rate by nZVI and Pd-nZVI in water confirm there is indeed a more than 30-fold increase in hydrogen evolution rate by doping the nanoparticles with a mass fraction of 1% of palladium (Table S1, Supporting Information). By approximating with a linear model of hydrogen generation with time, the life span of our Pd-nZVI nanoparticles is estimated to be approximately 38 h (Table S1). This figure is in good agreement with the observation that a sizable proportion of the aged Pd-nZVI had their metallic iron interior hollowed out after 24 h of aging in water.

**Implications for Water Remediation Applications.** nZVI-based bimetallic materials have been extensively studied for their enhanced reactivity and the generation of more benign end-products in the reductive dehalogenation of organic halides (Table 1). However, most studies have not considered the possibility of dynamic structural changes of the bimetallic nanoparticles in the aqueous reaction media. Structural characterization studies were typically performed on the fresh material, and it is assumed that the nanostructure and elemental distribution remain unchanged during the course of the remediation treatment. The observation that the Pd-Fe bimetallic nanoparticles can undergo massive structural and compositional changes in water over a time frame comparable to that of the contaminant transformation process calls for a significant modification of the reaction models of bimetallic nanoparticles. Enclosure of Pd by an extensive iron oxide layer due to aqueous aging clearly requires the contaminants (e.g., TCE) to penetrate into the particle and the products (e.g., ethane) to diffuse out through the oxide layer, which may affect reaction kinetics, alter the rate-limiting steps, and influence final product distributions. No detailed study has been performed yet on these aspects, but the apparent loss of reactivity for Pd-Fe materials after aging in water is observed in TCE batch experiments (Figure 7). The apparent reaction rate constant based on a pseudo-first-order reaction rate model decreased from  $5.7$   $\text{h}^{-1}$  for the fresh particles to  $0.96$   $\text{h}^{-1}$  upon 24 h aging. Decreased reaction rates have also been reported in prior studies over

repeated use of Pd–Fe particles in aqueous solutions (13), and these findings are consistent with the rapid enclosure of surface Pd sites by a growing iron oxide shell (Figures 4–6).

Prior studies have attempted to correlate the reactivity of the bimetallic particles with the mass loading of the additive metal. Instead of following a monotonically increasing trend, it has been observed that an optimal dosage exists and the reactivity declines with a further increase in the additive metal loading (2, 3, 29). The behavior may conceivably be attributable to accelerated particle aging and more rapid surface deactivation with increasing Pd dopant level. This hypothesis needs to be confirmed by systematically extending this study to Pd–Fe nanoparticles with different Pd contents. Differences in the initial structure of nZVI, the doping procedure, and the aging medium (for instance, in solvent/water mixture) may also affect the reactivity and aging of the bimetallic nanoparticles.

With regards to the potential application of bimetallic nanoparticles for in situ treatment of halogenated contaminants, our results imply that particle age and storage environment will play a critical role in determining the effectiveness of the remediation. For field applications of the palladized nZVI, palladium should be introduced onto the nZVI at the time of use due to the high reactivity and limited life span of Pd–nZVI. It has been noted that the presence of dissolved silica may slow down iron corrosion by adsorbing to the anodic surface (30). It may be the case that, in actual field applications, the life span of Pd–nZVI in a soil matrix containing silica and other corrosion inhibitors may be longer as compared to the life times in pure water studied here. On the other hand, Pd in the aged particles is embedded in the growing oxide phase and there is no dislodging of Pd metal or elution of Pd(II) ions into the aqueous phase. This attribute is highly favorable for the collection and recycling of palladium material and for addressing concerns regarding possible palladium leaching into the environment.

## Acknowledgments

A.A.H. and C.J.K. gratefully acknowledge funding from the NASA-Lehigh Nanotechnology Partnership. A.A.H. would also like to acknowledge the NRC postdoctoral associateship program. This work was partially supported by grants awarded to W.-X. Zhang by the U.S. Environmental Protection Agency (EPA STAR Grants R829625 and GR832225) and National Science Foundation of China (NSFC 50928802). The authors also acknowledge support of this work by the Pennsylvania Infrastructure Technology Alliance (PITA).

## Supporting Information Available

Detailed descriptions of experimental procedures. Figure S1 shows HAADF and STEM-XEDS images of fresh undoped nZVI. Figure S2 shows additional STEM-XEDS images of fresh Pd–nZVI. Table S1 tabulates the laboratory estimated hydrogen generation rates of nZVI and Pd–nZVI and their estimated life spans. This information is available free of charge via the Internet at <http://pubs.acs.org/>.

## Literature Cited

- Alonso, F.; Beletskaya, I. P.; Yus, M. Metal-mediated reductive hydrodehalogenation of organic halides. *Chem. Rev.* **2002**, *102*, 4009–4091.
- Cwiertny, D. M.; Bransfield, S. J.; Livi, K. J. T.; Fairbrother, D. H.; Roberts, A. L. Exploring the influence of granular iron additives on 1,1,1-trichloroethane reduction. *Environ. Sci. Technol.* **2006**, *40*, 6837–6843.
- Lien, H. L.; Zhang, W. X. Nanoscale Pd/Fe bimetallic particles: Catalytic effects of palladium on hydrodechlorination. *Appl. Catal. B* **2007**, *77*, 110–116.
- Lien, H. L.; Zhang, W. X. Transformation of chlorinated methanes by nanoscale iron particles. *J. Environ. Eng.* **1999**, *125*, 1042–1047.
- Zhang, W. X.; Wang, C. B.; Lien, H. L. Treatment of chlorinated organic contaminants with nanoscale bimetallic particles. *Catal. Today* **1998**, *40*, 387–395.
- Xu, J.; Dozier, A.; Bhattacharyya, D. Synthesis of nanoscale bimetallic particles in polyelectrolyte membrane matrix for reductive transformation of halogenated organic compounds. *J. Nanopart. Res.* **2005**, *7*, 449–467.
- He, F.; Zhao, D. Y.; Liu, J. C.; Roberts, C. B. Stabilization of Fe-Pd nanoparticles with sodium carboxymethyl cellulose for enhanced transport and dechlorination of trichloroethylene in soil and groundwater. *Ind. Eng. Chem. Res.* **2007**, *46*, 29–34.
- Korte, N. E.; Zutman, J. L.; Schlosser, R. M.; Liang, L.; Gu, B.; Fernando, Q. Field application of palladized iron for the dechlorination of trichloroethene. *Waste Manage.* **2000**, *20*, 687–694.
- Elliott, D. W.; Zhang, W. X. Field assessment of nanoscale bimetallic particles for groundwater treatment. *Environ. Sci. Technol.* **2001**, *35*, 4922–4926.
- Graham, L. J.; Jovanovic, G. Dechlorination of p-chlorophenol on a Pd/Fe catalyst in a magnetically stabilized fluidized bed; Implications for sludge and liquid remediation. *Chem. Eng. Sci.* **1999**, *54*, 3085–3093.
- Wang, C. B.; Zhang, W. X. Synthesizing nanoscale iron particles for rapid and complete dechlorination of TCE and PCBs. *Environ. Sci. Technol.* **1997**, *31*, 2154–2156.
- Choi, H.; Al-Abed, S. R.; Agarwal, S.; Dionysiou, D. D. Synthesis of reactive nano-Fe/Pd bimetallic system-impregnated activated carbon for the simultaneous adsorption and dechlorination of PCBs. *Chem. Mater.* **2008**, *20*, 3649–3655.
- Zhu, B. W.; Lim, T. T. Catalytic reduction of chlorobenzenes with Pd/Fe nanoparticles: reactive sites, catalyst stability, particle aging, and regeneration. *Environ. Sci. Technol.* **2007**, *41*, 7523–7529.
- Wong, M. S.; Alvarez, P. J. J.; Fang, Y. I.; Akcin, N.; Nutt, M. O.; Miller, J. T.; Heck, K. N. Cleaner water using bimetallic nanoparticle catalysts. *J. Chem. Technol. Biot.* **2009**, *84*, 158–166.
- Cheng, I. F.; Fernando, Q.; Korte, N. Electrochemical dechlorination of 4-Chlorophenol to Phenol. *Environ. Technol.* **1997**, *31*, 1074–1078.
- Liu, Y. Q.; Lowry, G. V. Effect of particle age (Fe-o content) and solution pH on NZVI reactivity: H-2 evolution and TCE dechlorination. *Environ. Sci. Technol.* **2006**, *40*, 6085–6090.
- Sarathy, V.; Tratnyek, P. G.; Nurmi, J. T.; Baer, D. R.; Amonette, J. E.; Chun, C. L.; Penn, R. L.; Reardon, E. J. Aging of iron nanoparticles in aqueous solution: Effects on structure and reactivity. *J. Phys. Chem. C* **2008**, *112*, 2286–2293.
- Muftikian, R.; Nebesny, K.; Fernando, Q.; Korte, N. X-ray photoelectron spectra of the palladium-iron bimetallic surface used for the rapid dechlorination of chlorinated organic environmental contaminants. *Environ. Sci. Technol.* **1996**, *30*, 3593–3596.
- Burke, M. G.; Watanabe, M.; Williams, D. B.; Hyde, J. M. Quantitative characterization of nanoprecipitates in irradiated low-alloy steels: advances in the application of FEG-STEM quantitative microanalysis to real materials. *J. Mater. Sci.* **2006**, *41*, 4512–4522.
- Herzing, A. A.; Watanabe, M.; Edwards, J. K.; Conte, M.; Tang, Z. R.; Hutchings, G. J.; Kiely, C. J. Energy dispersive X-ray spectroscopy of bimetallic nanoparticles in an aberration corrected scanning transmission electron microscope. *Faraday Discuss.* **2008**, *138*, 337–351.
- Watanabe, M.; Ackland, D. W.; Burrows, A.; Kiely, C. J.; Williams, D. B.; Krivanek, O. L.; Dellby, N.; Murfit, M. F.; Szilagyi, Z. Improvements in the X-ray analytical capabilities of a scanning transmission electron microscope by spherical-aberration correction. *Microsc. Microanal.* **2006**, *12*, 515–526.
- Available from <http://www.nist.gov/lispix/>.
- Martin, J. E.; Herzing, A. A.; Yan, W. L.; Li, X. Q.; Koel, B. E.; Kiely, C. J.; Zhang, W. X. Determination of the oxide layer thickness in core-shell zerovalent iron nanoparticles. *Langmuir* **2008**, *24*, 4329–4334.
- Li, X. Q.; Zhang, W. X. Sequestration of metal cations with zerovalent iron nanoparticles - A study with high resolution X-ray photoelectron spectroscopy (HR-XPS). *J. Phys. Chem. C* **2007**, *111*, 6939–6946.
- Carpenter, E. E.; Calvin, S.; Stroud, R. M.; Harris, V. G. Passivated iron as core-shell nanoparticles. *Chem. Mater.* **2003**, *15*, 3245–3246.

- (26) Wang, C. M.; Baer, D. R.; Thomas, L. E.; Amonette, J. E.; Antony, J.; Qiang, Y.; Duscher, G. Void formation during early stages of passivation: Initial oxidation of iron nanoparticles at room temperature. *J. Appl. Phys.* **2005**, *98*, 094308.
- (27) Yin, Y. D.; Rioux, R. M.; Erdonmez, C. K.; Hughes, S.; Somorjai, G. A.; Alivisatos, A. P. Formation of hollow nanocrystals through the nanoscale Kirkendall effect. *Science* **2004**, *304*, 711–714.
- (28) Bard, A. J.; Parsons, R.; Jordan, J.; Eds. *Standard Potentials in Aqueous Solution*; M. Dekker: New York, 1985.
- (29) Nutt, M. O.; Hughes, J. B.; Wong, M. S. Designing Pd-on-Au bimetallic nanoparticle catalysts for trichloroethene hydrodechlorination. *Environ. Sci. Technol.* **2005**, *39*, 1346–1353.
- (30) Reardon, E. J.; Fagan, R.; Vogan, J. L.; Przepiora, A. Anaerobic corrosion reaction kinetics of nanosized iron. *Environ. Sci. Technol.* **2008**, *42*, 2420–2425.

ES100051Q